nature structural & molecular biology

Single-molecule stepping and structural dynamics of myosin X

Yujie Sun[1], Osamu Sato[2], Felix Ruhnow[3], Mark E Arsenault[1], Mitsuo Ikebe[2] & Yale E Goldman[1]

Myosin X is an unconventional myosin with puzzling motility properties. We studied the motility of dimerized myosin X using the single-molecule fluorescence techniques polTIRF, FIONA and Parallax to measure the rotation angles and three-dimensional position of the molecule during its walk. It was found that Myosin X steps processively in a hand-over-hand manner following a left-handed helical path along both single actin filaments and bundles. Its step size and velocity are smaller on actin bundles than individual filaments, suggesting myosin X often steps onto neighboring filaments in a bundle. The data suggest that a previously postulated single α-helical domain mechanically extends the lever arm, which has three IQ motifs, and either the neck-tail hinge or the tail is flexible. These structural features, in conjunction with the membrane- and microtubule-binding domains, enable myosin X to perform multiple functions on varied actin structures in cells.

Myosin X, an unconventional member of the myosin superfamily, is widely expressed in vertebrate tissues. It is found to localize primarily to regions with dynamic actin reorganization, such as the tips of filopodia, the edges of lamellipodia and membrane ruffles[1–8]. At these actin-rich protrusions, myosin X plays a role in filopodia formation, extension and sensing, possibly by transporting actin-binding proteins to the tips and by linking membranes and actin[2–6,9,10]. Myosin X also interacts with mitotic spindle poles in *Xenopus laevis* oocytes and is important in maintenance of spindle integrity[11–14].

The intriguing cellular functions of myosin X are accomplished through its unique structural features: a motor domain, three calmodulin-binding IQ motifs, a putative single α-helical domain, a coiled coil and a tail containing three PH domains, one MyTH4 domain and one FERM domain per heavy chain[1]. The PH domains are unique among the myosin superfamily and enable myosin X to directly bind to the plasma membrane[2] and thereby mediate membrane-cytoskeleton interactions[4]. The MyTH4-FERM domain enables myosin X to interact with microtubules[11].

The *in vivo* and *in vitro* motility characteristics of myosin X are puzzling. Actin-based motility of various constructs has suggested that this myosin forms a dimer in the cell and moves processively toward the barbed ends of actin filaments[2,3,15]. However, the putative coiled-coil domain of myosin X is highly charged and unable to dimerize[16], so dimerization of myosin X might require other cellular components, as has been suggested for myosin VI (ref. 17). The kinetics of myosin X are also under debate[8,18]. Myosin X selects bundled actin for motility and shows poor processivity on single actin filaments[7]. However, myosin X has been found to interact with single actin filaments and possibly to move processively to carry cargoes or pull cytoskeletal filaments together[13,15,18,19]. Overall, mechanistically relevant information about the motility of myosin X, such as its processivity, step size and strain-dependent properties, is still largely in question.

In the present work, we used single-molecule polarized total internal reflection fluorescence (polTIRF) microscopy[20–23], fluorescence imaging with one-nanometer accuracy (FIONA)[24] and Parallax, a technique for nanometer-scale tracking of single fluorophores in three dimensions[25], to study the motility of a dimer construct of myosin X on actin filaments and bundles. We observed robust processivity of myosin X on single actin filaments and found that actin bundle formation is not required for processive movement, in contrast to previous results[7]. Myosin X walks hand over hand along actin filaments with a step size of 34 nm and has a left-handed helical path. It moves more slowly and has a smaller average step size on actin bundles than on single actin filaments, again following a left-handed helical path. The radii of the helical paths on actin filaments and bundles suggest a flexible tail or head-tail junction, and the step-size measurements support the hypothesis of an α-helical extension to the lever arm. These dynamic features and the diversified binding domains in its tail allow myosin X to interact with multiple binding targets and perform widely varied functions in crowded, actin-rich regions of the cell.

RESULTS

Myosin X moves processively on both actin filaments and bundles

A recombinant bovine myosin X HMM construct, dimerized by the myosin V coiled coil (Myo10-HMM-M5cc)[15,18,19], was used in most of the experiments. Myo10-HMM-M5cc was labeled either with bifunctional rhodamine (BR) on one of the calmodulin (CaM) subunits (termed MyoX-BRCaM), with a quantum dot (QD655, Invitrogen) on a CaM subunit in the lever arm (termed MyoX-LA-QD655), or with a quantum dot at the C terminus of the heavy chain (termed MyoX-CT-QD655). Single-molecule motility assays showed that myosin X moves processively on both single actin filaments and fascin-actin bundles, with characteristic run lengths of about 1 μm both at low (0.5 μM) and saturating (2 mM) Mg-ATP concentrations, and when

[1]Pennsylvania Muscle Institute, University of Pennsylvania, Philadelphia, Pennsylvania, USA. [2]University of Massachusetts Medical School, North Worcester, Massachusetts, USA. [3]Max Planck Institute of Molecular Cell Biology and Genetics, Dresden, Germany. Correspondence should be addressed to Y.E.G. (goldmany@mail.med.upenn.edu).

Received 18 June 2009; accepted 3 February 2010; published online 4 April 2010; doi:10.1038/nsmb.1785

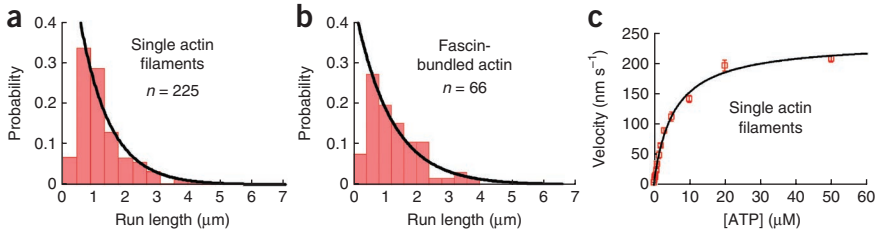

Figure 1 Processivity and stepping rates of labeled myosin X (MyoX-LA-QD655) actin filaments and actin bundles. (**a**) The run-length distribution on suspended actin filaments. A single exponential fit (the first bin is excluded from the fitting) gives an average run length of 0.95 μm (95% confidence limits, +0.25 μm and –0.16 μm). (**b**) The run-length distribution on surface-bound actin bundles. A single exponential fit (first bin excluded) gives an average run length of 1.16 μm (95% confidence limits, +0.28 μm and –0.16 μm). (**c**) Mg-ATP dependence of the velocity of single MyoX-LA-QD655 molecules on single immobilized actin filaments. Error bars are s.e.m. of the velocity.

actin was either bound to the surface or suspended above a 2-μm gap across microfabricated polymer ridges (**Fig. 1a**,**b**, **Supplementary Movies 1** and **2** and **Supplementary Table 1**). Therefore, immobilization of actin filaments or bundles onto the microscope slide does not appreciably decrease the processivity of myosin X. The stepping rate of myosin X depends on ATP concentration (**Fig. 1c**), leading to rate constants for ATP binding (k_{ATP+}) of 1.24 μM^{-1} s^{-1} and for an ATP-independent step (presumably ADP release, k_{ADP-}) of 6.90 s^{-1}. These values were one-half to one-third of those previously obtained for the single-headed construct[18], probably owing to temperature differences in the experiments and interhead tension (gating) in the dimer molecule, as previously shown for myosin VI (ref. 26).

The construct used for the experiments above was forced to dimerize by inclusion of the myosin V coiled-coil tail (M5cc) in its sequence. To test whether the artificial dimerization altered the motility relative to a more native construct, we also investigated the motility of green fluorescent protein (GFP)-tagged myosin X HMM, which does not spontaneously dimerize *in vitro*[2,3,15]. Following experiments on myosin VI (ref. 17), we tested whether bringing monomeric GFP–myosin X HMM molecules close to each other by binding to actin filaments in the absence of ATP would initiate their dimerization. Native myosin X monomers did dimerize as a result of proximity and, when ATP was subsequently added, moved processively along actin (**Supplementary Fig. 1** and **Supplementary Movie 3**). Most of the remaining data were obtained from a construct containing the M5cc tail, which facilitates dimerization but has motility similar to the native proximity-induced dimer.

Myosin X walks hand over hand with a 34-nm step size

In a polTIRF experiment, the BR in a MyoX-BRCaM molecule is excited by an evanescent field that has time-multiplexed polarizations. The polarized fluorescence intensities in a cycle of excitation polarizations are used to compute the orientation of the BR, defined by the axial angle β (probe polar angle relative to the actin axis) and α (probe azimuthal angle around actin)[20,22,27]. Single-molecule polTIRF recordings of MyoX-BRCaM at 2 μM Mg-ATP show the fluorescence intensities detected by the *x* and *y* polarized photon counters for each excitation polarization (**Supplementary Fig. 2a**). Abrupt changes of photon counts per detection interval in the individual polarized fluorescence intensity traces, without substantial change of the total photon-counting rate, indicate that the labeled lever arm tilts during processive motility, as shown by the corresponding β and α traces (**Fig. 2a**).

The distribution of β angles of all moving myosin X molecules ($n = 180$) has two peaks, at 42° and 135° (**Fig. 2b**), suggesting that the stepping of myosin X involves two states, as seen in the polTIRF results for myosin V (ref. 23) and myosin VI (ref. 20). If the probe dipole is out of the plane of the lever-arm tilting, the probe azimuth (α) will tilt during a step, even if the molecule walks straight along actin. About 90% of the step transitions of β and α occurred simultaneously, with approximately equal numbers showing correlated (increase of β with increase of α, and decrease of β with decrease of α; second half of the traces in **Fig. 2a**) or anticorrelated (first half of the traces in **Fig. 2a**) transitions. It is probably due to ambiguity from the twofold symmetry of the probe dipole of BR that the numbers of correlated and anticorrelated transitions are nearly equal[20,27].

If a myosin head alternates between leading and trailing positions, then the lever arm returns to its original state after two steps. In that circumstance, α will return to its former value after two steps if the molecule is walking straight, regardless of whether the probe is oriented in the tilting plane or not. The change of α after two steps, termed $^2\Delta\alpha$, can thus be used to evaluate whether the motor walks straight along the axis of actin[20]. The $^2\Delta\alpha$ distribution of myosin X (**Fig. 2c**), centered near 0, is approximately as narrow as that of myosin V (**Supplementary Fig. 2b**) and about half as wide as that of myosin VI (ref. 20). These results indicate that myosin X, like myosin V, steps mostly straight, in contrast to the chaotic side-to-side motions of myosin VI (ref. 20).

High-precision single-molecule tracking of fluorophores (FIONA, ref. 24) on the lever arms of myosin V (ref. 24) and VI (refs. 28,29) has shown that these isoforms step in a hand-over-hand manner, on the basis of the observation of alternating larger and smaller displacements of the fluorophore. We observed a similar stepping pattern of MyoX-LA-QD655 (**Fig. 3**). Clear alternating

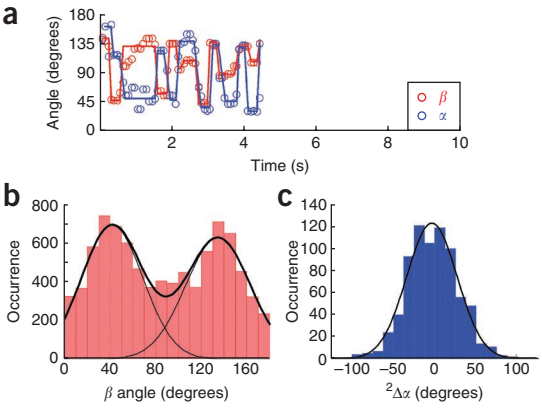

Figure 2 polTIRF results for MyoX-BRCaM stepping on an actin filament immobilized on the glass surface. (**a**) A typical time course of β (red, the axial angle of the BR probe relative to actin) and α (blue, the azimuthal angle of the probe around actin) transitions during myosin X motility at 2 μM Mg-ATP. Solid traces are Stepfinder fits[47] to the angle recordings. (**b**) The distribution of β angles. The two Gaussian fits (42 ± 27° (s.d., $n = 4{,}755$) and 135 ± 28° (s.d., $n = 3{,}948$)) suggest that the myosin X lever arm switches between leading and trailing states. (**c**) Distribution of the changes of α after two consecutive steps (same-state angular change), $^2\Delta\alpha$ (–3.4 ± 30° (s.d., $n = 757$)).

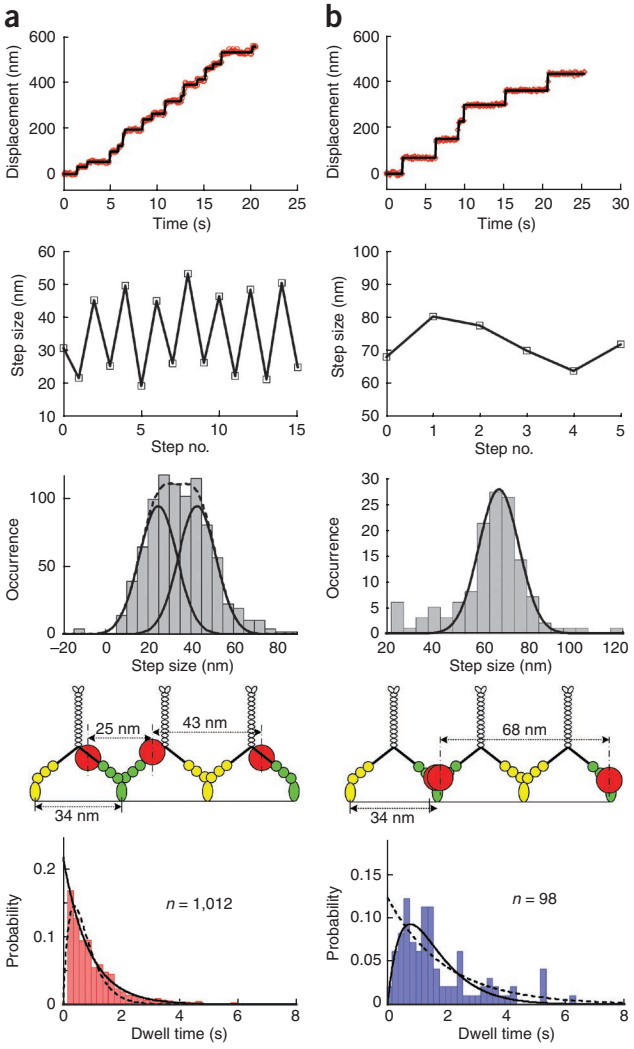

Figure 3 Alternating step size supports the hand-over-hand model of myosin X. (**a**) About 86% of MyoX-LA-QD655 molecules showed alternating larger and smaller displacements. The step sizes in the second panel are measured from the molecule of the first panel. The third panel shows the step-size histogram of 66 alternating molecules. It is fitted with two Gaussian components of equal amplitude and width (solid curves, 25 ± 9.4 nm and 43 ± 9.4 nm (s.d.); the dashed curve is the sum of the two solid curves). Alternating large and small steps are expected if the quantum dot is on the third CaM, as shown in the cartoon in the fourth panel. The dwell-time distribution (fifth panel, red bars) is fitted by a single exponential $P(t) = ke^{-kt}$, yielding an average waiting time ($1/k$) of 0.89 s at 1 μM Mg-ATP. The dashed curve is a double exponential that doesn't approximate the data as well (*F*-test). (**b**) The rest of the MyoX-LA-QD655 molecules (14%) showed larger step sizes of 68 ± 8.4 nm (s.d., $n = 142$). This behavior is expected if the quantum dot is on the first CaM, as shown in the cartoon in the fourth panel. The dwell-time distribution for the 0- to 68-nm case, blue bars, is fitted by a convolution of two single exponentials, $P(t) = tk^2e^{-kt}$, yielding an average waiting time ($2/k$) of 1.62 s at 1 μM Mg-ATP, about double the waiting time for the 25- to 43-nm case. The dashed curve is a poorer fit by a single exponential decay (*F*-test).

~25-nm and ~45-nm displacements were observed for 86% of myosin X molecules (**Fig. 3a**, top two panels). The rest of the MyoX-LA-QD655 molecules showed larger step sizes with a narrower distribution, at 68 ± 8.4 nm (s.d.; **Fig. 3b**).

The step-size distribution of the alternating molecules (middle panel of **Fig. 3a**) could be fitted by a single Gaussian curve at 34 ± 14 nm (s.d.). However, owing to the clear alternation of step sizes in these molecules (typical recordings are shown in top two panels of **Fig. 3a**), which produces two populations of steps in equal numbers, we fit the distribution with two Gaussian components having equal areas (amplitudes and s.d. of the two components were forced to be equal). The fitting yielded peaks centered at 25 nm and 43 nm, which, in conjunction with the relatively large size of the quantum dot (~15 nm), suggest that the quantum dot is probably located on the second or third CaM in these molecules (cartoon panel of **Fig. 3a**). The average of the two alternating step sizes suggests that myosin X's center of mass translocates about 34 nm on each step. This interpretation is confirmed by the step-size measurements of MyoX-CT-QD655 (**Fig. 4**), which indicate the motion of the tail of the molecule, tracking the center of mass.

The myosin X molecules producing 68-nm steps probably have a quantum dot located on the first CaM and thus alternated between 0- and 68-nm steps (cartoon panel of **Fig. 3b**). Since 0-nm steps are not discernible, each observed 68-nm step is limited by two consecutive events, the steps of the labeled and unlabeled heads. The dwell-time distributions of the two types of myosin X (bottom of **Fig. 3**) strongly support that interpretation. The dwell-time distribution for the 25- to 43-nm molecules (red bars in **Fig. 3a**, bottom) can be fitted by a single exponential $P(t) = ke^{-kt}$, consistent with the labeled and unlabeled heads having the same stepping rate. The dwell-time distribution for the 0- to 68-nm molecules (blue bars in **Fig. 3b**, bottom) is fitted better by the convolution of two exponentials $P(t) = tk^2e^{-kt}$, as expected from two reactions with equal rates in series[24]. These results strongly support the hand-over-hand model of myosin X processivity.

Processive motility shows quantitative differences on fascin-actin bundles compared to single actin filaments. Myosin X moves about 26% faster on actin filaments than on fascin-actin bundles at low

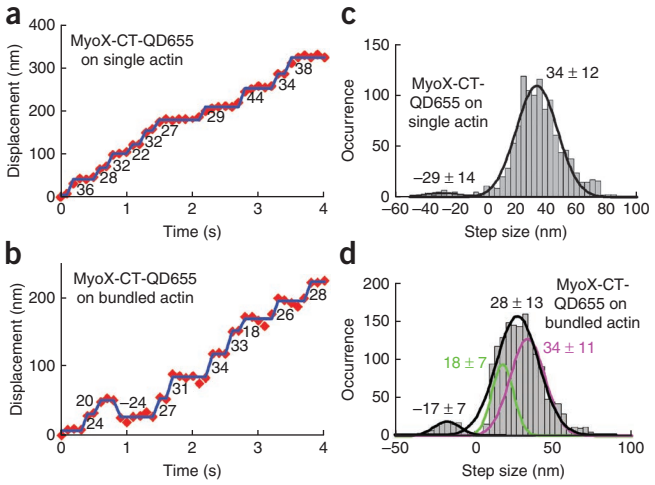

Figure 4 MyoX-CT-QD655 shows different stepping behavior along actin filaments and bundles. (**a**) A stepping trace of myosin X on a single actin filament. (**b**) A stepping trace of myosin X on an actin bundle. (**c**) The step-size distribution of MyoX-CT-QD655 on actin filaments with mostly forward steps (34 ± 14 nm, s.d., $n = 1,105$) and 4.5% backward steps (–29 ± 14 nm, s.d., $n = 53$). (**d**) The step-size distribution of MyoX-CT-QD655 on actin bundles with mostly forward steps (28 ± 13 nm, s.d., $n = 1,349$) and 8% backward steps (–17 ± 7 nm, s.d., $n = 113$), fitted with black curves. The data of forward steps were also fitted with two Gaussian components (magenta and green curves), with the center of the magenta curve fixed at 34 nm for comparison with **c**. Mg-ATP concentration was 2 μM.

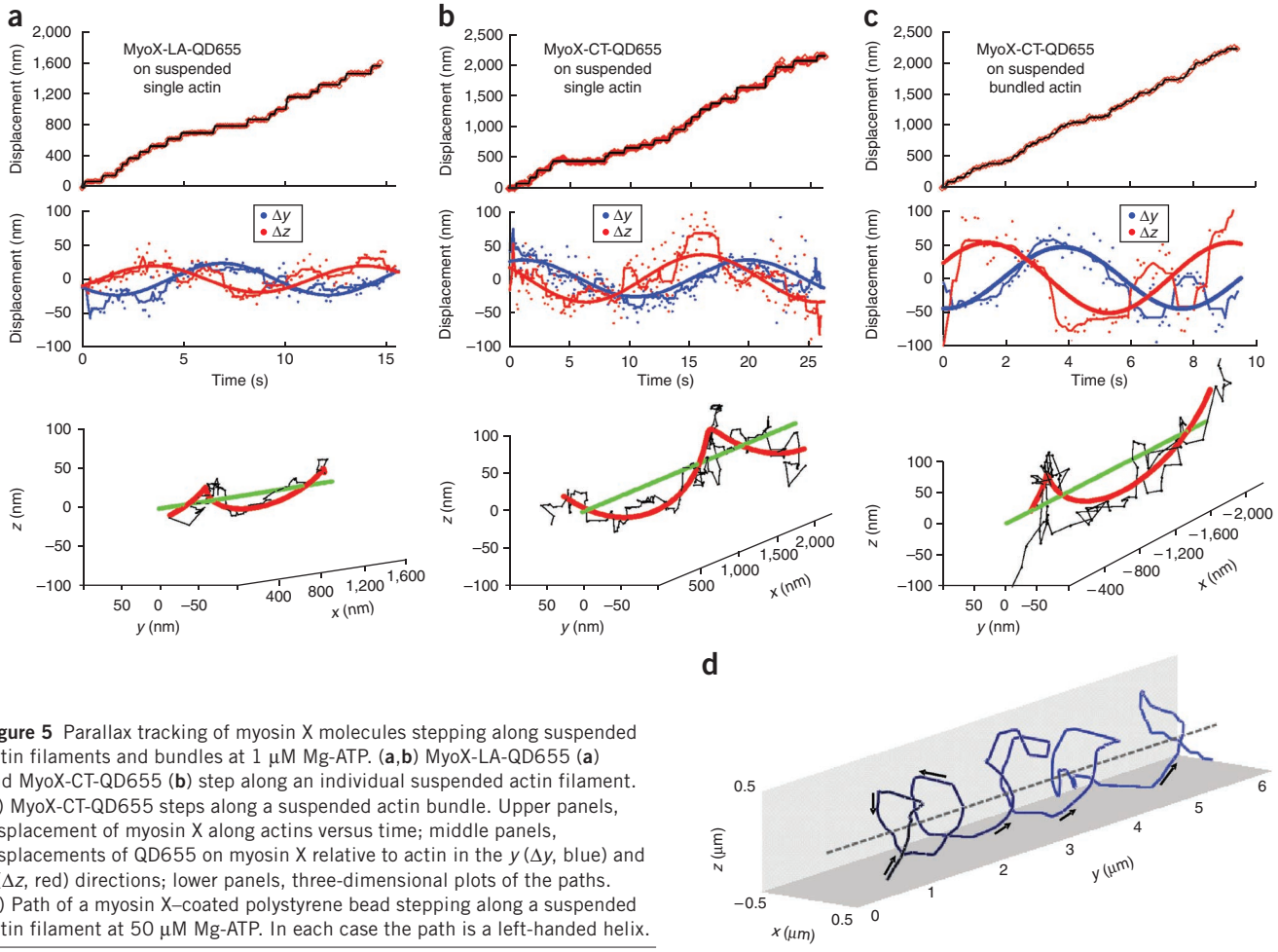

Figure 5 Parallax tracking of myosin X molecules stepping along suspended actin filaments and bundles at 1 μM Mg-ATP. (**a**,**b**) MyoX-LA-QD655 (**a**) and MyoX-CT-QD655 (**b**) step along an individual suspended actin filament. (**c**) MyoX-CT-QD655 steps along a suspended actin bundle. Upper panels, displacement of myosin X along actins versus time; middle panels, displacements of QD655 on myosin X relative to actin in the *y* (Δ*y*, blue) and *z* (Δ*z*, red) directions; lower panels, three-dimensional plots of the paths. (**d**) Path of a myosin X–coated polystyrene bead stepping along a suspended actin filament at 50 μM Mg-ATP. In each case the path is a left-handed helix.

and saturating ATP concentrations (Mg-ATP at 0.5 μM–2 mM, **Supplementary Table 1**). On bundled actin, the center of mass of myosin X (tracked on MyoX-CT-QD655) showed a smaller average step size (27 nm, including backward steps; **Fig. 4d**) than that on single filaments (34 nm, **Fig. 4c**), which can be attributed partly to more backward steps (8.0% of all steps on bundled actin, compared with 4.5% on single filaments) and partly to a higher proportion of short steps (~20 nm) on bundled actin (**Fig. 4d**). The ratio of the average step size (including short and backward steps) on single filaments to the average step size on bundled actin is 1.26, consistent with the difference in myosin X velocities. The average size of myosin X's backward steps is also different on bundled actin (17 nm, **Fig. 4d**) compared to single filaments (29 nm, **Fig. 4c**).

To test whether these differences in velocity and back-stepping are caused by polarity variations of the actin within bundles, we characterized the fascin-bundled actin using transmission electron microscopy (Online Methods and **Supplementary Fig. 3**). The number of filaments per bundle was found to be 8.5 ± 0.4 and the actin center-to-center spacing in the bundle was 10.6 ± 0.1 nm (s.e.m., $n = 39$ bundles). Decoration of the actin filaments in bundles with myosin II MgSubfragment-1 (**Supplementary Fig. 3c**,**d**) showed that all of the filaments in the bundles are polarized in the same direction ($n = 18$ bundles), consistent with a previous report[30]. Therefore, the backward steps observed were not the result of myosin X switching onto filaments with opposite polarity. Rather, the stepping dynamics suggest that myosin X takes long, straight steps along individual actin filaments in bundles but sometimes steps sideways onto a neighboring filament in the bundle, producing a smaller step, either forward or backward.

We also measured the velocity of native myosin V on actin bundles and single actin filaments at 1 μM and 500 μM Mg-ATP. At both ATP concentrations, myosin V moves about 36% faster on single actin filaments than on bundles, which is due to more short steps on bundles (**Supplementary Fig. 4**). Nevertheless, myosin V produces fewer backward steps than myosin X on both types of track.

Myosin X walks in a left-handed helical path along actin

The 34-nm step size suggests that the trailing and leading heads of myosin X bind actins separated by 11 (31 nm) and 13 (36 nm) actin monomers, respectively. For these spans, the myosin molecules would not be subjected to high intramolecular strain that would occur as a result of large azimuthal differences between other pairs of actin binding sites[20,31,32]. Stepping on the eleventh and thirteenth actin monomers, myosin X should have a net left-handed twirling path along actin[33]. In conventional *in vitro* processive motility assays, though, actin is usually fixed onto a substratum so that the myosin molecules cannot access the space underneath the actin, preventing full rotations of helical motion.

We suspended actin filaments and bundles over microfabricated trenches (**Supplementary Fig. 5**) and used the Parallax technique[25] to study the three-dimensional motion of myosin X. The microstructures were rows of polymethylmethacrylate ridges and grooves at 3-μm pitch. The grooves were measured to be 2 μm wide and 350 nm deep by

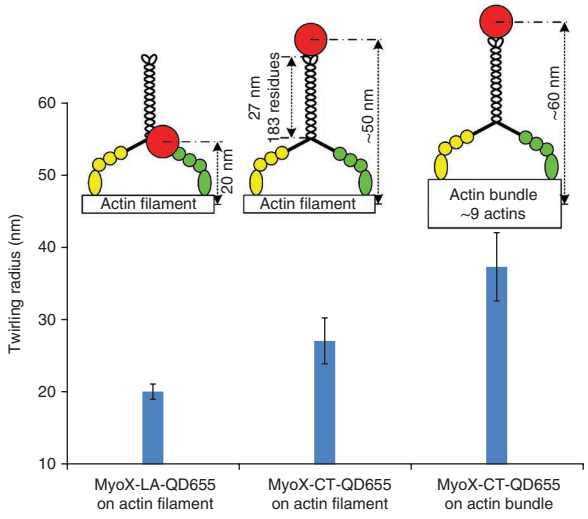

Figure 6 Radial amplitudes of helical paths of myosin X molecules stepping along suspended actins. The cartoons are drawn approximately to scale to show the expected amplitudes of the QD655 helical paths in the three cases. The measured amplitude increases in the examples from left to right, but not as much as would be expected if the motor tail were straight and oriented radially. Error bars are s.e.m. of the radii.

contact mode atomic force microscopy (**Supplementary Fig. 5b**). Actin was suspended over the grooves and pulled taut by hydrodynamic flow (Online Methods). Images with TIRF and low-angle oblique illumination[34] confirmed that most of the filaments were suspended away from the slide surface (**Supplementary Fig. 5**).

MyoX-LA-QD655 (**Fig. 5a**) and MyoX-CT-QD655 (**Fig. 5b**,**c**) were observed stepping along suspended actin filaments and fascin-actin bundles (**Supplementary Movie 2**). In **Figure 5a–c**, each upper panel shows the displacement of myosin X along the actin aligned with the *x* direction in the microscope, and each middle panel shows the lateral displacement of the quantum dot relative to the actin in the *y* (blue) and *z* (red) directions. The lateral displacements are fitted with sinusoidal functions to obtain their periods, amplitudes and phases. The lower panels are three-dimensional plots of the *x*, *y* and *z* displacements. The green line represents the actin position, the black traces are the trajectories of myosin X relative to actin, and the red trace represents the sinusoidal fitted path. In all three examples, the *z* displacement leads the *y* displacement by approximately a quarter of a period, which indicates that the paths are left-handed helices.

Of 465 MyoX-LA-QD655 and MyoX-CT-QD655 molecules moving on suspended actin filaments, 308 (66%) followed helical paths around actin, the rest traveling approximately straight over their run lengths. In contrast, on actin bundles, only 28% of MyoX-CT-QD655 molecules showed helical motion; most of the molecules walked straight. The mean helical pitches in the three cases are all close to 1 μm (MyoX-LA-QD655 on actin filaments, 1,018 ± 37 nm (s.e.m., $n = 225$); MyoX-CT-QD655 on actin filaments, 1,042 ± 67 nm (s.e.m., $n = 83$); MyoX-CT-QD655 on actin bundles, 1,037 ± 49 nm (s.e.m., $n = 11$)), which is slightly smaller than the value, 1,296 nm, expected from the step size of 34 nm[35]. This difference is probably due to the average run length of myosin X (**Fig. 1** and **Supplementary Table 1**) being similar to its helical pitch, causing many short runs with long helical pitches not to show periodic deflections and thus excluding them from the pitch analysis. To quantify the pitch, we included only molecules whose run length was one-half of a helical turn or more. Myosin X may also have a longer true helical pitch on bundled actin than on single filaments so that many molecules dissociated from actin before they finished moving half of their helical path, and thus were categorized into the group of straight-walkers. This effect would result in fewer helically walking molecules on bundles (28%) than on single filaments (66%).

The mean radii of the helical paths were substantially different for the two labeling positions and between actin filaments and bundles (**Fig. 6**). The path of the probe of MyoX-LA-QD655 on actin filaments had a radius of 20.1 ± 1.0 nm (s.e.m., $n = 225$), approximately the value expected, as illustrated in the leftmost cartoon of **Figure 6**. The myosin V coiled coil (183 residues) between the head-tail junction and the C terminus of MyoX-CT-QD655 would extend the radius ~27 nm if it were straight (middle cartoon in **Fig. 6**). However, the radius of the probe path of MyoX-CT-QD655 on actin filaments was 27.1 ± 3.1 nm (s.e.m., $n = 83$), only 7 nm greater than that of MyoX-LA-QD655, suggesting that the coiled coil is not straight or oriented radially, presumably owing to flexibility at the head-tail junction or farther along the sequence. The helical radius of MyoX-CT-QD655 on bundles of approximately nine actin filaments was 37.4 ± 4.7 nm (s.e.m., $n = 11$), 10 nm larger than that on individual filaments, which is reasonably consistent with the increased radius of the bundles (rightmost cartoon in **Fig. 6**). We also measured the path of polystyrene beads (1 μm diameter, Polysciences), heavily coated with myosin X, along actin filaments that we had suspended between gold electrodes using dielectrophoresis in an alternating-current electric field[36,37]. Myosin X–coated beads followed left-handed helical paths with a pitch of 1.5 ± 0.4 μm (s.d., $n = 4$) (**Fig. 5d**).

DISCUSSION

Our results show that myosin X moves processively on individual actin filaments, with an average step size of 34 nm, and more slowly on actin bundles, with an average step size of 27 nm. A processive myosin motor requires a high duty ratio and a sufficiently long lever arm to stride between appropriately oriented binding sites on the helical actin track. The myosin X construct used in this study has been found to have a high duty ratio[18], although a bovine myosin X S1 construct produced a low duty ratio[8]. This discrepancy has been discussed previously[18]. The robust processivity reported here implies a high duty ratio in our construct.

Each myosin X lever arm has three IQ motifs (extending about 10.8 nm), so a myosin X dimer would be expected to stride maximally over 22 nm if there were no further extension to its lever arm or unraveling of its proximal tail. It has been suggested[16] that the proximal tail domains of myosin X form nondimerizing stable single α-helices (SAH domains) that act as mechanically stiff extensions to the myosin X lever arm. The SAH sequence (55 residues following the third IQ motif) and the distal coiled-coil domain (the next 78 residues) are both present in the construct mainly used here, followed by the coiled-coil domain from myosin V to force dimerization.

The 34-nm step size of myosin X on actin filaments (**Figs. 3** and **4**) supports the assumption that there are extensions to the lever arm of myosin X beyond the 10.8-nm length of its three CaM binding sites. The postulated 55-residue SAH domain may increase the length of lever arm by approximately 7.5 nm[16] and allow the two heads of myosin X to bind 11 or 13 actin monomers apart, in sterically favorable configurations.

Myosin VI is another myosin motor that is thought to have extensions to its lever arms and thereby reach a large step size[20,26,38]. However, evidence from different measurements, including angles and step sizes, suggests there are differences in the rigidity of the lever arms of myosin V, myosin VI and myosin X. The change of the probe azimuthal angle α after two steps, $^2\Delta\alpha$, is related to the

path of a moving myosin motor[20]. The $^2\Delta\alpha$ distribution of myosin VI has been found to be much wider ($\sigma = 55°$)[20] than that of myosin V ($\sigma = 29°$, **Supplementary Fig. 2b**) or myosin X ($\sigma = 30°$, **Fig. 2c**), suggesting that myosin VI has more flexible lever arms and walks more 'wiggly' on actin filaments[20]. The step-size distributions of the three myosin motors are consistent with these angular measurements. The stepping distance of fluorescently labeled myosin X heads (twice the center-of-mass motion, 68 ± 8.4 nm (s.d., $n = 1,168$); **Fig. 3b**) has variability closer to that of myosin V (74 ± 5.3 nm, s.d., in ref. 24; 74 ± 7.7 nm, s.d., $n = 140$, in **Supplementary Fig. 4a**), than to myosin VI (70 ± 23 nm, s.d.[28]). The higher variability in the step size of myosin VI is probably due to its high flexibility. Lever-arm flexibility may also affect the likelihood of backward steps. Myosin VI has more backward steps[29,39] than myosin V (ref. 24 and **Supplementary Fig. 4**). In our step-size measurements on myosin X (**Fig. 4**) and myosin V (**Supplementary Fig. 4**), we found that myosin X also has more backward steps than myosin V.

The differences in the lever-arm rigidity of the three myosins are a consequence of their structures. Myosin V has rigid lever arms with six bound CaMs and produces robust processive stepping. To achieve their large step sizes, however, both myosin VI and myosin X need extensions to their short lever arms, which seem to increase the overall flexibility. Part of the extended myosin VI lever arm may contain a random coil[20,26,29] or an unfolded three-helix bundle[38], which confers high flexibility. In contrast, myosin X has only one SAH to extend its three-CaM bound lever arm. The SAH is expected to be less rigid than the lever arm of myosin V but more rigid than the extension of myosin VI. Thus, the SAH domain of myosin X is likely to carry mechanical load and facilitate intramolecular gating[40]. Further evidence has been reported[41] that the SAH domain can extend the functional length of myosin lever arms, irrespective of gating.

Myosin X moves more slowly on fascin-actin bundles than it does on actin filaments, consistent with its smaller average step size of 27 nm on bundled actins (**Fig. 4c**,**d**). The variable step sizes and left-handed helical walking path of myosin X on actin bundles (**Figs. 5** and **6**) suggest that myosin X switches onto adjacent actin filaments rather randomly. This contrasts with a proposed more predictable 'straddle mechanism'[7], in which the two heads of a myosin X necessarily track along two adjacent actin filaments. Our measurements show that myosin V also moves more slowly on actin bundles than on single filaments. The multiple actin binding sites available in a bundle seem to deflect myosin V and myosin X from a straight path, producing slower velocities. Nevertheless, it may be advantageous that myosin X is able to switch onto adjacent actin filaments in a bundle or span between two actin filaments. For instance, this feature may allow myosin X to bypass 'road blocks' on actin bundles during cargo transport in a crowded filopodia. Myosin X is able to pull actin filaments together at the cell periphery to initiate filopodial actin bundles[15], implying that myosin X can span across actin filaments.

Processive motility after dimerization of the native tail sequence by clustering on actin shows that processive motility of myosin X on individual actin filaments is a feature of the native molecule when two motor domains are paired. The robust processivity we observed on individual actin filaments contrasts with a report[7] that myosin X preferentially selects bundled actins for motility and shows poor processivity on single filaments. These differences are presumably due to the different truncation points in the coiled-coil domain or dimerization sequences and positions used in the two studies. The myosin X construct of ref. 7 uses a GCN4 leucine zipper to ensure dimerization of the heavy chains rather than the myosin V tail used here. The GCN4 was placed in almost the same position (19 residues earlier) as the start of our myosin V tail. The stability and flexibility of the putative SAH domain may depend on details or the position of the following coiled coil, and an unstable domain structure might diminish gating within myosin X. Alternatively, it is plausible that a leucine zipper might decrease the flexibility of the neck for finding appropriate binding sites on actin filaments, thus reducing the processivity. The radii of helical paths for CaM-labeled and C-terminally labeled myosin X (**Figs. 5** and **6**) imply that the tail of our construct is flexible.

Myosin X has been found to walk on both individual actin filaments[13,15,18,19] and actin bundles[7] in cells, as we observed *in vitro*. The postulated cellular functions of myosin X are surprisingly varied, probably requiring bivalent association with different actin filaments in the formation of filopodia[15], membrane interactions in the transport of integrins[4] and growth-factor receptors[3] to filopodial tips and in amplifying morphogenic signals[9], and possibly microtubule binding in maintenance of nuclear position and the mitotic or meiotic spindle[11–13]. The flexible tail or head-tail junction in myosin X may enable interactions between its head and tail domains to regulate its activity, like myosin V (refs. 42,43), and would also allow myosin X to adopt different geometries in complex, more or less dense actin structures in the lamellipodia and filopodia, and near the nucleus and the spindle. The semiflexible nature of the SAH domains and tail may allow myosin X to stretch, to pull multiple actin filaments into bundles at the base of filopodia[15] and to squeeze through narrow cytoplasmic spaces during transport in the cell body or filopodia. It is conceivable that a myosin X carrying integrins or other cargoes into a filopodium would adopt a spiral motion to ensure location of a substrate for attachment.

Conversion of nonprocessive monomers into processive dimers has been observed for myosin VI and postulated to be a regulatory feature of other myosins[17,44–46]. Our observation that native myosin X monomers are not processive but undergo proximity-induced dimerization and thereby become processive provides support for that postulate. The monomer-dimer conversion may regulate the local cellular function of myosin X as a structural anchor or a cargo transporter.

In this study, we used the single-molecule fluorescence techniques polTIRF, FIONA and Parallax to investigate the motility of myosin X on actin filaments and bundles. Myosin X moved processively on both single actin filaments and bundles in a hand-over-hand manner. On actin bundles, myosin X often switched tracks onto adjacent actin filaments and had slower velocity than on single filaments. The trajectories of myosin X moving freely around suspended actins followed left-handed helical paths, consistent with the 34-nm step size. Our data support the hypothesis of single α-helical extensions to the lever arms and suggest a flexible head-tail junction. These structural and dynamical features provide myosin X the adaptability needed for moving and binding on different structures of the actin cytoskeleton and for its highly varied cellular functions.

METHODS

Methods and any associated references are available in the online version of the paper at http://www.nature.com/nsmb/.

Note: Supplementary information is available on the Nature Structural & Molecular Biology website.

ACKNOWLEDGMENTS

We acknowledge discussion and comments by J.H. Lewis and J.F. Beausang. We thank T.M. Svitkina and C. Yang for characterization of fascin-bundled actin by electron microscopy (US National Institutes of Health (NIH) grant RR 22482) and K. Homma (University of Massachusetts Medical School) for the GFP–Myosin X HMM construct. Bifunctional rhodamine (BR-I2) was a generous gift from J.E.T. Corrie (UK Medical Research Council National Institute for Medical Research).

This work was supported by US National Science Foundation Nanoscale Science and Engineering Center grant DMR-0425780 through the Nano/Bio Interface Center and NIH grant GM086352.

AUTHOR CONTRIBUTIONS

Y.S. carried out the single-molecule experiments and data analysis. O.S. prepared and labeled the myosin X protein. F.R. coded Matlab scripts for analysis of FIONA data. M.E.A. carried out the bead motility assay on suspended filaments and data analysis. M.I. and Y.E.G. supervised the project and, with Y.S., wrote the manuscript.

COMPETING FINANCIAL INTERESTS

The authors declare no competing financial interests.

Published online at http://www.nature.com/nsmb/.
Reprints and permissions information is available online at http://npg.nature.com/reprintsandpermissions/.

1. Berg, J.S., Derfler, B.H., Pennisi, C.M., Corey, D.P. & Cheney, R.E. Myosin-X, a novel myosin with pleckstrin homology domains, associates with regions of dynamic actin. *J. Cell Sci.* **113**, 3439–3451 (2000).
2. Berg, J.S. & Cheney, R.E. Myosin-X is an unconventional myosin that undergoes intrafilopodial motility. *Nat. Cell Biol.* **4**, 246–250 (2002).
3. Tokuo, H. & Ikebe, M. Myosin X transports Mena/VASP to the tip of filopodia. *Biochem. Biophys. Res. Commun.* **319**, 214–220 (2004).
4. Zhang, H. *et al.* Myosin-X provides a motor-based link between integrins and the cytoskeleton. *Nat. Cell Biol.* **6**, 523–531 (2004).
5. Sousa, A.D. & Cheney, R.E. Myosin-X: a molecular motor at the cell's fingertips. *Trends Cell Biol.* **15**, 533–539 (2005).
6. Bohil, A.B., Robertson, B.W. & Cheney, R.E. Myosin-X is a molecular motor that functions in filopodia formation. *Proc. Natl. Acad. Sci. USA* **103**, 12411–12416 (2006).
7. Nagy, S. *et al.* A myosin motor that selects bundled actin for motility. *Proc. Natl. Acad. Sci. USA* **105**, 9616–9620 (2008).
8. Kovacs, M., Wang, F. & Sellers, J.R. Mechanism of action of myosin X, a membrane-associated molecular motor. *J. Biol. Chem.* **280**, 15071–15083 (2005).
9. Zhu, X.-J. *et al.* Myosin X regulates netrin receptors and functions in axonal path-finding. *Nat. Cell Biol.* **9**, 184–192 (2007).
10. Pi, X. *et al.* Sequential roles for myosin-X in BMP6-dependent filopodial extension, migration, and activation of BMP receptors. *J. Cell Biol.* **179**, 1569–1582 (2007).
11. Weber, K.L., Sokac, A.M., Berg, J.S., Cheney, R.E. & Bement, W.M. A microtubule-binding myosin required for nuclear anchoring and spindle assembly. *Nature* **431**, 325–329 (2004).
12. Toyoshima, F. & Nishida, E. Integrin-mediated adhesion orients the spindle parallel to the substratum in an EB1- and myosin X-dependent manner. *EMBO J.* **26**, 1487–1498 (2007).
13. Woolner, S., O'Brien, L.L., Wiese, C. & Bement, W.M. Myosin-10 and actin filaments are essential for mitotic spindle function. *J. Cell Biol.* **182**, 77–88 (2008).
14. Wühr, M., Mitchison, T.J. & Field, C.M. Mitosis: new roles for myosin-X and actin at the spindle. *Curr. Biol.* **18**, R912–914 (2008).
15. Tokuo, H., Mabuchi, K. & Ikebe, M. The motor activity of myosin-X promotes actin fiber convergence at the cell periphery to initiate filopodia formation. *J. Cell Biol.* **179**, 229–238 (2007).
16. Knight, P.J. *et al.* The predicted coiled-coil domain of myosin 10 forms a novel elongated domain that lengthens the head. *J. Biol. Chem.* **280**, 34702–34708 (2005).
17. Park, H. *et al.* Full-length myosin VI dimerizes and moves processively along actin filaments upon monomer clustering. *Mol. Cell* **21**, 331–336 (2006).
18. Homma, K. & Ikebe, M. Myosin X is a high duty ratio motor. *J. Biol. Chem.* **280**, 29381–29391 (2005).
19. Homma, K., Saito, J., Ikebe, R. & Ikebe, M. Motor function and regulation of myosin X. *J. Biol. Chem.* **276**, 34348–34354 (2001).
20. Sun, Y. *et al.* Myosin VI walks "wiggly" on actin with large and variable tilting. *Mol. Cell* **28**, 954–964 (2007).
21. Forkey, J.N., Quinlan, M.E. & Goldman, Y.E. Protein structural dynamics by single-molecule fluorescence polarization. *Prog. Biophys. Mol. Biol.* **74**, 1–35 (2000).
22. Rosenberg, S.A., Quinlan, M.E., Forkey, J.N. & Goldman, Y.E. Rotational motions of macromolecules by single-molecule fluorescence microscopy. *Acc. Chem. Res.* **38**, 583–593 (2005).
23. Forkey, J.N., Quinlan, M.E., Shaw, M.A., Corrie, J.E.T. & Goldman, Y.E. Three-dimensional structural dynamics of myosin V by single-molecule fluorescence polarization. *Nature* **422**, 399–404 (2003).
24. Yildiz, A. *et al.* Myosin V walks hand-over-hand: single fluorophore imaging with 1.5-nm localization. *Science* **300**, 2061–2065 (2003).
25. Sun, Y., Dawicki McKenna, J.M., Murray, J.M., Ostap, E.M. & Goldman, Y.E. Parallax: high accuracy three-dimensional single molecule tracking using split images. *Nano Lett.* **9**, 2676–2682 (2009).
26. Rock, R.S. *et al.* A flexible domain is essential for the large step size and processivity of myosin VI. *Mol. Cell* **17**, 603–609 (2005).
27. Beausang, J.F., Sun, Y., Quinlan, M.E., Forkey, J.N. & Goldman, Y.E. Single molecule fluorescence polarization via polarized total internal reflection fluorescent microscopy. in *Single-Molecule Techniques: A Laboratory Manual* (eds. Selvin, P.R. & Ha, T.) 121–148 (Cold Spring Harbor Laboratory, Cold Spring Harbor, New York, USA, 2007).
28. Ökten, Z., Churchman, L.S., Rock, R.S. & Spudich, J.A. Myosin VI walks hand-over-hand along actin. *Nat. Struct. Mol. Biol.* **11**, 884–887 (2004).
29. Yildiz, A. *et al.* Myosin VI steps via a hand-over-hand mechanism with its lever arm undergoing fluctuations when attached to actin. *J. Biol. Chem.* **279**, 37222–37226 (2004).
30. Ishikawa, R., Sakamoto, T., Ando, T., Higashi-Fujime, S. & Kohama, K. Polarized actin bundles formed by human fascin-1: their sliding and disassembly on myosin II and myosin V *in vitro*. *J. Neurochem.* **87**, 676–685 (2003).
31. Vilfan, A. Elastic lever-arm model for myosin V. *Biophys. J.* **88**, 3792–3805 (2005).
32. Lan, G. & Sun, S.X. Flexible light-chain and helical structure of F-actin explain the movement and step size of myosin-VI. *Biophys. J.* **91**, 4002–4013 (2006).
33. Beausang, J.F., Schroeder, H.W. III, Nelson, P.C. & Goldman, Y.E. Twirling of actin by myosins II and V observed via polarized TIRF in a modified gliding assay. *Biophys. J.* **95**, 5820–5831 (2008).
34. Sako, Y., Minoguchi, S. & Yanagida, T. Single-molecule imaging of EGFR signalling on the surface of living cells. *Nat. Cell Biol.* **2**, 168–172 (2000).
35. Ali, M.Y. *et al.* Myosin V is a left-handed spiral motor on the right-handed actin helix. *Nat. Struct. Biol.* **9**, 464–467 (2002).
36. Arsenault, M.E., Sun, Y., Bau, H.H. & Goldman, Y.E. Using electrical and optical tweezers to facilitate studies of molecular motors. *Phys. Chem. Chem. Phys.* **11**, 4834–4839 (2009).
37. Arsenault, M.E., Zhao, H., Purohit, P.K., Goldman, Y.E. & Bau, H.H. Confinement and manipulation of actin filaments by electric fields. *Biophys. J.* **93**, L42–L44 (2007).
38. Mukherjea, M. *et al.* Myosin VI dimerization triggers an unfolding of a three-helix bundle in order to extend its reach. *Mol. Cell* **35**, 305–315 (2009).
39. Rock, R.S. *et al.* Myosin VI is a processive motor with a large step size. *Proc. Natl. Acad. Sci. USA* **98**, 13655–13659 (2001).
40. Choe, S. & Sun, S.X. The elasticity of α-helices. *J. Chem. Phys.* **122**, 244912 (2005).
41. Baboolal, T.G. *et al.* The SAH domain extends the functional length of the myosin lever. *Proc. Natl. Acad. Sci. USA* **106**, 22193–22198 (2009).
42. Li, X.-D., Jung, H.S., Mabuchi, K., Craig, R. & Ikebe, M. The globular tail domain of myosin Va functions as an inhibitor of the myosin Va motor. *J. Biol. Chem.* **281**, 21789–21798 (2006).
43. Thirumurugan, K., Sakamoto, T., Hammer, J.A. III, Sellers, J.R. & Knight, P.J. The cargo-binding domain regulates structure and activity of myosin 5. *Nature* **442**, 212–215 (2006).
44. Yu, C. *et al.* Myosin VI undergoes cargo-mediated dimerization. *Cell* **138**, 537–548 (2009).
45. Phichith, D. *et al.* Cargo binding induces dimerization of myosin VI. *Proc. Natl. Acad. Sci. USA* **106**, 17320–17324 (2009).
46. Iwaki, M. *et al.* Cargo-binding makes a wild-type single-headed myosin-VI move processively. *Biophys. J.* **90**, 3643–3652 (2006).
47. Kerssemakers, J.W. *et al.* Assembly dynamics of microtubules at molecular resolution. *Nature* **442**, 709–712 (2006).

ONLINE METHODS

Expression, purification and labeling of myosin X. We expressed and purified native myosin X (including residues 1–979) and recombinant myosin X constructs, Myo10-HMM-M5cc (for MyoX-LA-QD655) and Myo10-HMM-M5cc-BAP (for MyoX-CT-QD655), in SF9 cells as described previously[15,18,19]. The native myosin X has His and Flag tags at the N terminus, followed by a GFP motif (GFP–Myosin X HMM). We performed biotinylation of Myo10-HMM-M5cc-BAP on the Flag resin using 0.01 mg ml^{-1} biotin protein ligase (Avidity, LLC) in a solution containing 50 mM bicine, pH 8.3, 10 mM ATP, 10 mM magnesium acetate, 50 μM biotin and 1 mM DTT on ice overnight. For polTIRF experiments, we labeled myosin X with bifunctional rhodamine on calmodulin (CAM) (BR-I2, a generous gift from J.E.T. Corrie[48], as was done previously for myosin V (ref. 24) and myosin VI (ref. 20).

In separate experiments, we labeled myosin X with streptavidin-coated quantum dots QD655 (Invitrogen) via biotin-streptavidin linkage to a CaM or the C terminus of the heavy chain. We prepared biotinylated CaM (biotin-CaM) with P66C chicken CaM mutation[23] and biotin-maleimide (Sigma) essentially as described[49].

Actin filaments and fascin-actin bundles. We purified G-actin from rabbit skeletal muscle as described[50]. We prepared Alexa647-labeled F-actin (G-actin/Alexa647 ratio of 5:1) and rhodamine-phalloidin–labeled F-actin as described previously[20,27]. We expressed and purified fascin in SF9 cells[51]. We prepared actin bundles by mixing and incubating 3 μM fascin and 8 μM F-actin on ice for 2 d[7].

Single-molecule polTIRF assay. We prepared flow chambers by assembling a fused silica slide (Quartz Scientific) with a glass coverslip using double-sided adhesive tape. We immobilized actin on the surface by successive incubations with *N*-ethylmaleimide–treated myosin II (NEM-myosin II) (60 nM, 5 min) and Alexa647-labeled F-actin (100 nM, 1 min). We blocked the surface using 5 mg ml^{-1} casein (5 min). Finally, we introduced 100 pM BR-CaM–labeled myo10-HMM-M5cc in the motility buffer (M5Buffer: 25 mM KCl, 20 mM HEPES, pH 7.6, 5 mM $MgCl_2$, 1 mM EGTA, 10 mM DTT, 100 μg ml^{-1} wild-type CaM, 10 mM phosphocreatine (Sigma P-7936), 0.3 mg ml^{-1} creatine phosphokinase (prepared daily from powder, Sigma C-3755) and the desired amount of ATP).

In previous reports[20,22,27], we have described our single-molecule polTIRF setup, which allows unambiguous resolution of individual probe dipole orientations within a hemisphere. Temporal resolution here was 80 ms.

Single-molecule *in vitro* motility assay. We used an inverted Nikon TE-2000U microscope with objective-type (Nikon ×100, 1.49 NA objective) TIRF excitation from a solid-state 488-nm laser (Coherent), a solid-state 532-nm laser (CrystaLaser) and a back-illuminated electron multiplier–CCD (charge-coupled device) camera (Cascade-512B, Photometrics).

The flow chamber assembly and the immobilization of actin (filaments and bundles) were similar to that in the single-molecule polTIRF assay, except the fused silica slide was replaced by a glass slide. The motility mixture contained ~600 pM of QD655-labeled myosin X in M5Buffer and an oxygen scavenging system (glucose oxidase, catalase and glucose[52]).

Actin-assisted dimerization of myosin X HMM. To enable proximity-induced dimerization of native myosin X, we first immobilized 800 nM actin filaments on a flow chamber surface, precoated with NEM-myosin (30 nM) for 3 min. Then we added 200 nM GFP–myosin X HMM and incubated for 5 min in the absence of ATP. Lastly, we flowed in M5Buffer containing 10 μM ATP to wash out the unbound myosin X and initiate motility of myosin X dimers. We conducted control experiments by flowing 5 nM myosin X HMM into the flow chamber in the presence of 10 μM ATP. We quantified the number of myosin X molecules in moving fluorescent spots by comparing their GFP fluorescence intensity to that of monomeric myosin X, containing one GFP molecule, stuck on the surface.

Characterization of fascin-actin bundles. We used a transmission electron microscope (JEM 1011, JEOL USA) operated at 100 kV to characterize fascin-actin bundles, which were adhered to carbon-coated grids and negatively stained with uranyl acetate. For most of the actin bundles, we could identify individual filaments in the bundle (**Supplementary Fig. 3a**). Cross-linking fascin molecules were sometimes recognized as periodic densities (**Supplementary Fig. 3b**). We also investigated whether actin filaments are uniformly polarized within bundles by decorating with myosin II MgSubfragment-1 (**Supplementary Fig. 3c,d**).

Three-dimensional tracking on suspended actin filaments and bundles. We have developed a three-dimensional tracking technique, Parallax, based on a stereoscopic split-view of the sample, to track the motion of QD655-labeled myosin X molecules along suspended actin. The details of the Parallax setup and calibrations are described in ref. 25.

Myosin X is constrained from exploring all the way around surface-bound actin filaments. In the three-dimensional tracking experiments, we suspended actin filaments or bundles across microfabricated polymethylmethacrylate ridges so that there was clearance between the substrate and suspended actin (see **Supplementary Fig. 5**). We prepared the microstructures using a micromolding technique[25,53,54] (described in **Supplementary Fig. 5**).

To suspend actin filaments taut over the microfabricated structures, we added three successive 20-μl aliquots of actin (500 nM) into the chamber at intervals of 15 s. The high concentration and short incubation time caused many of the actin filaments to bind to the NEM-myosin–coated ridges as they were drawn across the pedestals by the flow. For both two- and three-dimensional single-molecule position data, we tracked the QD655-labeled myosin X using an in-house-written Matlab (Mathworks, Inc.) tracking program[55] or ImageJ[56] plug-in. For QD655 in Parallax tracking, the uncertainty (s.d.) of location was about 4 nm in the *x* and *y* directions and about 8 nm in the *z* direction at 100-ms sampling intervals.

Bead motility assay on suspended filaments. We used dielectrophoresis to stretch and suspend actin filaments across a trench etched between two gold electrodes[36,37]. We used optical tweezers to bring myosin X–coated polystyrene beads (Polysciences; myosin/bead ratio of 10^4:1) onto the suspended actin filaments in M5Buffer (with 50 μM Mg-ATP) and an oxygen scavenging system. The beads were able to move freely along and about the suspended filaments, and we tracked their three-dimensional positions using defocused images[36,37].

48. Corrie, J.E.T., Craik, J.S. & Munasinghe, V.R.N. A homobifunctional rhodamine for labeling proteins with defined orientations of a fluorophore. *Bioconjug. Chem.* **9**, 160–167 (1998).
49. Dunn, A.R. & Spudich, J.A. Dynamics of the unbound head during myosin V processive translocation. *Nat. Struct. Mol. Biol.* **14**, 246–248 (2007).
50. Pardee, J.D. & Spudich, J.A. Purification of muscle actin. *Methods Cell Biol.* **24**, 271–289 (1982).
51. Homma, K., Saito, J., Ikebe, R. & Ikebe, M. Ca^{2+}-dependent regulation of the motor activity of myosin V. *J. Biol. Chem.* **275**, 34766–34771 (2000).
52. Harada, Y., Sakurada, K., Aoki, T., Thomas, D.D. & Yanagida, T. Mechanochemical coupling in actomyosin energy transduction studied by in vitro movement assay. *J. Mol. Biol.* **216**, 49–68 (1990).
53. Michel, B. *et al.* Printing meets lithography: soft approaches to high-resolution printing. *IBM J. Res. Develop.* **45**, 697–719 (2001).
54. Schmid, H. & Michel, B. Siloxane polymers for high-resolution, high-accuracy soft lithography. *Macromolecules* **33**, 3042–3049 (2000).
55. Nitzsche, B., Ruhnow, F. & Diez, S. Quantum-dot-assisted characterization of microtubule rotations during cargo transport. *Nat. Nanotechnol.* **3**, 552–556 (2008).
56. Abramoff, M.D., Magelhaes, P.J. & Ram, S.J. Image processing with ImageJ. *Biophotonics Int.* **11**, 36–42 (2004).

doi:10.1038/nsmb.1785